Journal of Colloid and Interface Science 537 (2019) 716–724

Contents lists available at ScienceDirect

Journal of Colloid and Interface Science

journal homepage: www.elsevier.com/locate/jcis

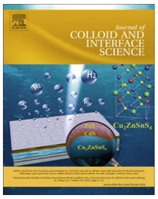

Editor's Choice

Heteroatom-doped carbon dots based catalysts for oxygen reduction reactions

Peng Zhang[a], Ji-Shi Wei[a], Xiao-Bo Chen[b], Huan-Ming Xiong[a,]*

[a] Department of Chemistry and Shanghai Key Laboratory of Molecular Catalysis and Innovative Materials, Fudan University, Shanghai 200433, PR China
[b] School of Engineering, RMIT University, Carlton, VIC 3053, Australia

GRAPHICAL ABSTRACT

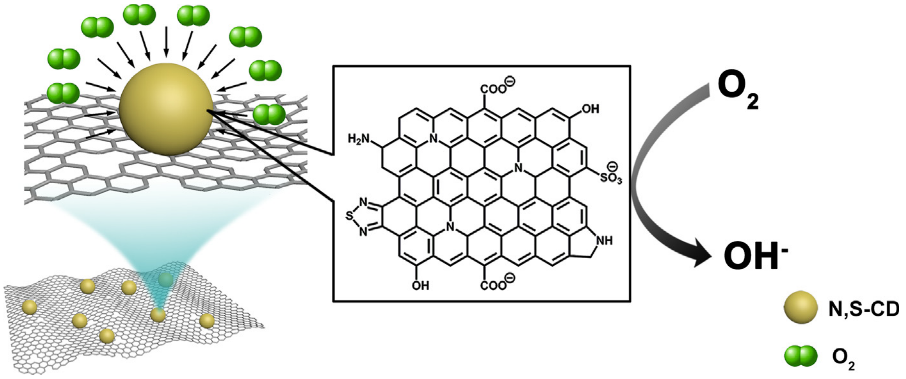

ARTICLE INFO

Article history:
Received 17 August 2018
Revised 5 November 2018
Accepted 8 November 2018
Available online 9 November 2018

Keywords:
Carbon dots
Doping
Electrocatalysis
Graphene
Oxygen reduction reaction

ABSTRACT

Carbon materials doped with heteroatoms are a class of cost-effective and stable electrocatalysts for oxygen reduction reactions (ORR), whose activities are mainly based on the heteroatom-related active sites. Besides the widely reported one-dimensional carbon nanotubes and two-dimensional graphene materials, carbon dots (CDs), as a new kind of zero-dimensional carbon materials, exhibit a range of unique structures and promising catalytic activities for ORR. In order to optimize the complex conditions of carbon-based catalysts, composites consisting of doped CDs and reduced graphene oxide (rGO) (designated as CD/rGO) are prepared hydrothermally, in comparison with directly doped rGO. All produced composites outperform their corresponding directly doped rGO counterparts in ORR measurements. It is noted that nitrogen and sulfur co-doped samples perform better than those doped by individual N or S. Mechanistic relationships between the ORR catalytic activities and the catalyst features are proposed, including type, location, bonding, fraction and synergistic effects of dopants, as well as the composition and structure of the carbon substrates. It is apparent that doping heteroatoms and constructing carbon substrates play a synergistic role in yielding high-performance carbon based catalysts.

1. Introduction

During the past decade, design and development of highly active catalysts for oxygen reduction reactions (ORR) have received extensive attention owing to their great potential for optimizing the performance of fuel cells and metal-air batteries [1–3]. A

---

* Corresponding author.
E-mail address: hmxiong@fudan.edu.cn (H.-M. Xiong).

https://doi.org/10.1016/j.jcis.2018.11.024

popular class of ORR electrocatalysts is heteroatom-doped carbon materials, based on pyrolytic carbon, carbon nanotubes, graphene and their derivatives [4–6], which possess lower cost and better stability than precious metal-based catalysts, such as Pt and Pd. Both experimental and theoretical studies have proved that heteroatom doping is a key factor that produces active catalytic sites and boosts ORR in these carbon materials [7]. In general, a practical doping state involves heteroatom types [8], dopant species with different bonding forms, and especially the locations and chemical environments of heteroatoms [9–11]. For example, active sites are usually more efficient at edges than those in planes of a catalyst, because the former are more exposed and easier to contact oxygen molecules [12–14]. In addition, the catalytic activity of a dopant are both determined by the dopants and the carbon substrates, and thus, it is an effective way to produce catalysts containing distinct ORR active sites through constructing a composite carbon material with doping heteroatoms preferentially on edges [15,16]. Carbon dots (CDs), as a new zero-dimensional carbon material with abundant edges, is a promising candidate for constructing ORR electrocatalysts with high activities.

History of CDs can be traced back to the discovery of fluorescent nanoparticles when separating carbon nanotubes, and thereafter they have been widely studied and applied in various fields including energy storage and conversion [17–20]. With diameters below 10 nm, abundant surface groups and various defects, CDs possess distinct electronic properties and high surface-volume ratios in comparison with 1-D carbon nanotubes and 2-D graphene, indicating that CDs have enormous space to produce a high density of ORR active sites [21–23]. CDs can be modified with various functional groups and doped with diverse chemical structures, which is favourable for the oxygen adsorption and reduction [24–26]. In general, CDs can be synthesized hydrothermally from small molecule precursors at relatively low temperatures. Doping CDs with heteroatoms such as N, S, B and P, etc., can be realized simultaneously just by adding dopant precursors into the preparation systems. Such a simple route can realize the doping and carbonization of CDs efficiently, and also endows CDs distinctive compositions with a large diversity of heteroatoms.

Though some pioneer work of CDs as ORR electrocatalysts [27–30] ascribed the superiority of CDs to their abundant edges and defects, their ORR activities in terms of their unique core-shell structures have not been fully studied. When CDs are fabricated from a mixture of organic molecules at a relatively low temperature, crystallization is confined within dimensions of a few nanometers, which facilitates the formation of graphitic cores and heteroatom-composed shells with various functional groups. In such a structure, the graphitic cores guarantee the electron conductivity, whilst the heteroatom dopants alter the electronic states of the adjacent carbon atoms to form active catalyzing sites on surface. This situation differs greatly from the doping states in other carbon materials. Hence, investigation on such distinctive chemical structures in CDs is key to elucidate the relationships between ORR activities and the structures of carbon materials.

In the present study, we synthesize N-doped CDs (N-CD), S-doped CDs (S-CD) and N,S-codoped CDs (N,S-CD) through similar hydrothermal reactions, respectively [31]. Afterwards, these CDs are anchored onto rGO sheets hydrothermally to form composites N-CD/rGO, S-CD/rGO and N,S-CD/rGO, respectively. For comparison, rGO samples are directly doped through a hydrothermal approach with the same doping agents to yield N-rGO, S-rGO and N,S-rGO, respectively. CD/rGO composites outperform their rGO counterparts in terms of electrochemical properties in ORR, which is attributed to their unique compositions and structures. Though either individual N or S dopants is able to give rise to active ORR sites in CDs and rGO, N,S-codoping is a more effective strategy to realize a four electron transfer pathway in ORR. As a result, optimal N,S-CD/rGO samples exhibit the most positive half-wave potential, the highest kinetic current density and the largest electron transfer number.

2. Experimental

2.1. Synthesis of CDs

N-CDs were synthesized using a classic method [32], whilst S-CDs and N,S-CDs were produced through a facile method based on our previous work [31]. For N-CDs, citric acid (3.07 g) and ethylenediamine (0.96 g) were dissolved in deionized water (30 mL); regarding S-CDs, NaOH (0.1 g) was dissolved in deionized water (50 mL) followed by adding α-lipoic acid (0.5 g); in terms of N,S-CDs, α-lipoic acid (0.5 g), NaOH (0.1 g) and ethylenediamine (0.3 g) were mixed into deionized water (50 mL). The above solutions were then transferred into respective Teflon-lined stainless steel autoclaves and heated at 180 °C for 24 h. After naturally cooling down to room temperature, the obtained solutions were purified by an analysis membrane (Spectrum, MW cutoff 3500) against water, respectively. Finally, three kinds of CDs aqueous solutions were freeze-dried respectively for subsequent experiments.

2.2. Preparation of CD/rGO composites

N-CD/rGO, S-CD/rGO and N,S-CD/rGO were also prepared hydrothermally. Firstly, GO was synthesized from graphite powder according to a modified Hummers method [33]. Then, GO (10 mg) was dispersed in deionized water (5 mL) followed by adding CDs (10 mg) under vigorous stirring. The mixture solution was continuously stirred for 2 h and transferred into a Teflon-lined stainless steel autoclave, then heated at 180 °C for 24 h. The products were separated and washed via centrifugation. For preparation of neat rGO controls, GO solution (5 mL, 2 mg/mL) was directly treated by the same hydrothermal method as the above mentioned procedure.

2.3. Preparation of directly doped rGO

rGO was doped directly in the same way as the above procedures. In brief, GO (10 mg) was dispersed in deionized water (5 mL), followed by addition of ethylenediamine (0.16 g), α-lipoic acid (30 mg) and NaOH (6 mg) under vigorous stirring. The mixture was continuously stirred at room temperature for 2 h, followed by heating at 180 °C for 24 h in a Teflon-lined stainless steel autoclave. The products were separated and washed via centrifugation and dried to yield N,S-rGO. For the case of N-rGO, the preparation procedure was the same as above, only free of α-lipoic acid and NaOH. For synthesizing S-rGO, similar experimental procedures were performed without involvement of ethylenediamine.

2.4. Electrochemical measurements

Electrochemical studies were performed at room temperature in a conventional three-electrode cell controlled through an electrochemical workstation (CH Instruments 660E, Chenhua Instr. Co., China). For cyclic voltammetry (CV) measurement, a glassy carbon (GC) electrode (3.0 mm in diameter) coated with catalyst inks was used as the working electrode. To prepare the catalyst inks, the well-ground powdered catalysts (5 mg) and Nafion (DuPont, 25 μL, 5%) were dispersed in of ethanol (1.0 mL) by ultrasonication. Afterwards, the catalyst inks (5 μL) was dropped onto the GC electrode and dried at room temperature. A saturated calomel electrode (SCE) and a Pt plate were used as reference and counter electrodes, respectively. All potentials referred in the paper were converted with a reference to the reversible hydrogen electrode (RHE) for convenience, calculated using the following equation:

$$E\ \text{vs.}\ RHE = E\ \text{vs.}\ SCE + 0.0591 \times pH + 0.241\ V$$

CV tests were performed in a N_2-saturated and O_2-saturated 0.1 M KOH solution at room temperature, respectively. The experiments were cycled at a scanning rate of 50 mV s^{-1} over the potential range from 0.15 to 1.15 V vs. RHE. For linear sweep voltammetry (LSV) measurements, a rotating disk electrode (RDE, 3.0 mm in diameter, Pine Research Instrumentation, USA) was used with rotating speeds varying from 100 to 2025 rpm (rounds per minute) at a scanning rate of 5 mV s^{-1} over the potential range from 0.9 to 0.2 V vs. RHE. RDE data were analyzed based on the Koutecky-Levich (K-L) equations:

$$\frac{1}{j} = \frac{1}{j_k} + \frac{1}{B\omega^{0.5}}$$

$$B = 0.62nF(D_{O_2})^{\frac{2}{3}}\upsilon^{-\frac{1}{6}}C_{O_2}$$

where j and j_k are the measured and kinetic current densities, respectively, and ω is the rotation speed. F is the Faraday constant (96,485 C mol^{-1}), and n is the number of electrons transferred in the reduction of one O_2 molecule, D is the diffusion coefficient of O_2 in 0.1 M KOH (1.9×10^{-5} cm^2 s^{-1}), C is the saturation concentration of O_2 in 0.1 M KOH (1.2×10^{-6} mol cm^{-3}), and ν is the kinematic viscosity of the electrolyte ($\nu = 0.01$ cm^2 s^{-1}). Koutecky-Levich plots were obtained at different potentials varying from 0.6 to 0.4 V vs. RHE, and the corresponding electron transfer numbers and kinetic current densities in the oxygen reduction reaction were calculated from slopes of the Koutecky-Levich plots.

3. Results and discussion

3.1. Parallel syntheses of CD/rGO composites and the directly doped rGO samples

Preparation procedures of N,S-CD/rGO composites and N,S-rGO are illustrated in Scheme 1. In brief, N,S-CDs were first synthesized using α-lipoic acid and ethylenediamine as respective sulfur and nitrogen sources. Then the as-prepared CDs and GO aqueous suspensions were mixed and hydrothermally treated for 24 h. In this procedure, GO was reduced into rGO by removing carbonyl and epoxy groups, and CDs were anchored onto rGO sheets. Two CD/rGO composites doped respectively with N and S were synthesized through similar procedures. The mass ratio of CDs and rGO was controlled at a proper value (1:1) because more CDs would reduce the electro-conductivity of composites and less CDs could not provide enough catalytic sites. rGOs doped with N, S or N,S were prepared with the same approach and precursors as those for CD/rGO composites. It should be mentioned that high-temperature calcination is often used to enhance the conductivity of carbon materials and produce active sites for high ORR performances [34,35]. But calcination will destroy CDs and induce unpredictable changes in both structures and compositions of the well-designed composites. In order to avoid any incomparable results, all treatments in the present research were conducted at a lower temperature, *i.e.* 180 °C, than those (700–1000 °C) in literature.

3.2. Morphologies and internal structures of CD/rGO composites and directly doped rGO samples

Morphologies of the CD/rGO composites were examined by transmission electron microscopy (TEM, Fig. 1a, c and e). It is apparent that a uniform and complete coverage of CDs exists on the surface of rGO, independent of dopants. In contrast, surface of directly doped rGO samples exhibits smooth and clean features (Fig. 1b, d and f). To verify the original morphology of CDs, TEM micrographs of free CDs are illustrated (Fig. S1a–c). CDs are uniformly and well dispersed, with a mean particle size of approx. 2 nm, in accordance with those presented in CD/rGO composites (Fig. 1a, c and e). Free rGO is also prepared and characterized by scanning electron microscopy (SEM) and TEM (Fig. S1d and e, respectively), revealing smooth and slightly wrinkled surface characteristics, and overlapping at the fringes (Fig. S1f). In contrast, TEM micrographs of N,S-CD/rGO, N-CD/rGO and S-CD/rGO (Fig. S2a–c) display more wrinkled and rougher surfaces. Regarding directly doped rGO (Fig. S2d–f), fewer and slighter wrinkles are apparent in surface than those of CD/rGO composites. From a larger scale perspective, N,S-CD/rGO composites exhibit porous and winkled structures (Fig. 1g and h, S3 and S4), whilst the directly doped rGO samples show flat surface features. The nitrogen physisorption measurements (Fig. S5) also prove that N,S-CD/rGO has a larger specific surface area (289.54 m^2 g^{-1}) than N,S-rGO (76.06 m^2 g^{-1}). These results indicate that the incorporation of CDs contribute greatly to the structural changes and an increase of edges in CD/rGOs that can improve ORR performance [36].

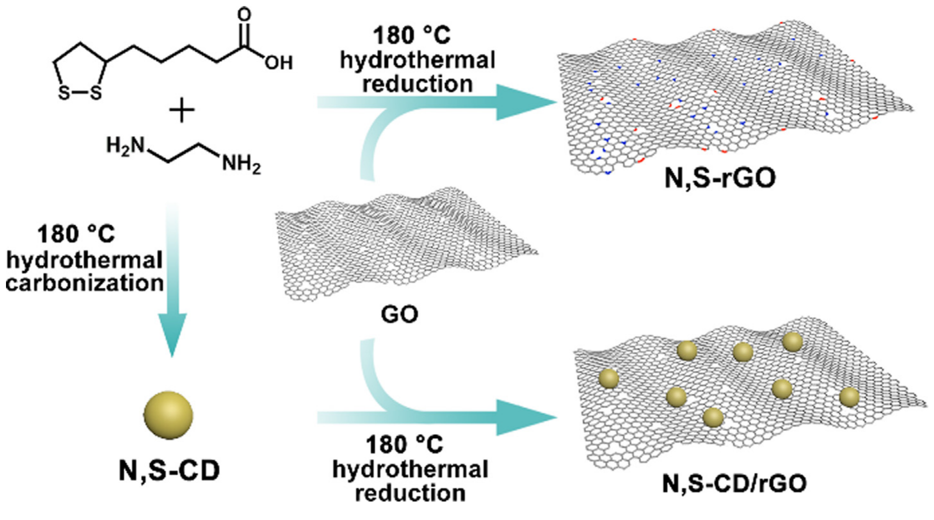

Scheme 1. Schematic illustration of the preparation procedures of N,S-CD/rGO composites and N,S-rGO controls.

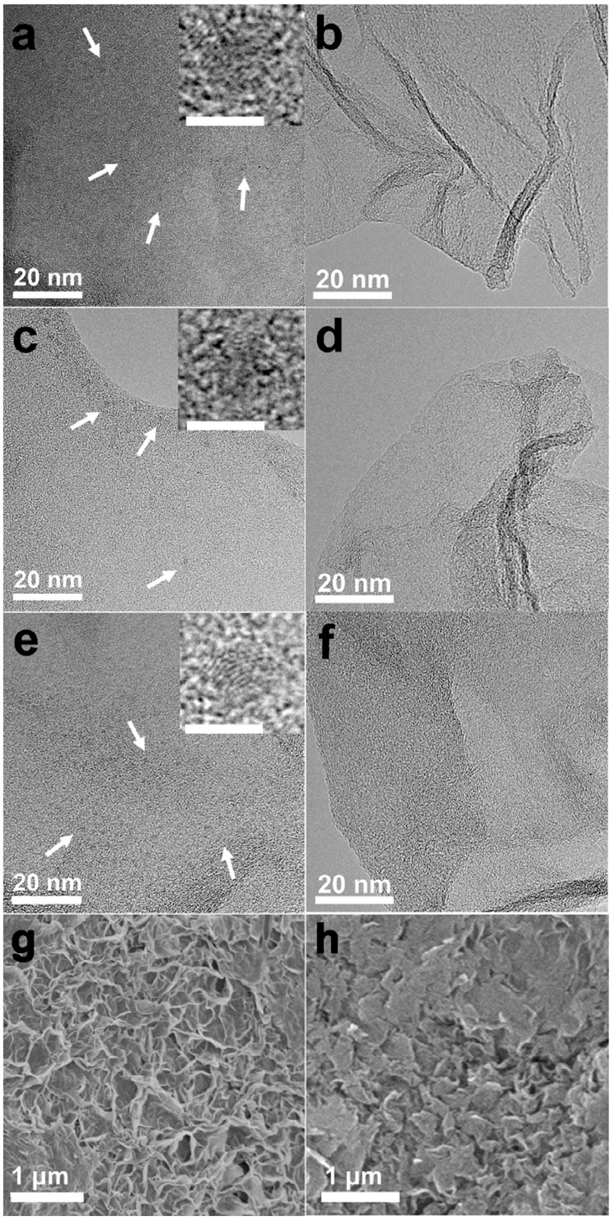

Fig. 1. TEM images of (a) N,S-CD/rGO, (b) N,S-rGO, (c) N-CD/rGO, (d) N-rGO, (e) S-CD/rGO and (f) S-rGO; (g) SEM images of N,S-CD/rGO and (h) N,S-rGO. The inset pictures are HRTEM images indicating one individual representative rGO decorated with CDs, as marked by white arrows. The scale bars in the insets represent 2 nm.

XRD patterns of CD/rGO composites and directly doped rGO are illustrated in Fig. 2a and b, respectively. Two broad peaks at about 25° and 44° are observed for all samples, corresponding to the (0 0 2) and (1 0 0) diffractions of the graphitic carbon structures [37]. XRD peaks of the doped samples (both CD/rGOs and directly doped rGOs) are broader than that of free rGO, owing to the disordered structures derived from heteroatom doping.

To elucidate doping effects on CDs, Raman spectra were recorded to determine the defect ratios (Fig. 2c and d). It reveals that two distinctive peaks around 1340 and 1580 cm^{-1} correspond to D band and G band, respectively. D band is associated with the disordered sp^2 carbon structure of graphene, while G band is ascribed to the typical E_{2g} stretching mode of C=C bond in graphitic materials. I_D/I_G value is widely recognized indicator of the disorder degree of carbon materials [38]. After CDs were loaded onto rGO, I_D/I_G value increases from 2.19 (rGO) to 2.31 (N-CD/rGO), and 2.24 (S-CD/rGO), indicating the presence of heteroatom-doped CDs in rGO. Given the highest I_D/I_G value (2.37), N,S-CD/rGO exhibits the most disordered structure of all prepared samples, which can be ascribed to a synergistic effect of N and S co-doping. Regarding the directly doped rGO samples in Fig. 2d, N,S-rGO also presents the most defective structure with the highest I_D/I_G value (2.26 for N,S-rGO, 2.25 for N-rGO and 2.21 for S-rGO). It is evident that I_D/I_G values of all directly doped rGO samples are lower than those of their CD/rGO counterparts, implying that the incorporation of CDs contribute greatly to the disordered structures of CD/rGO composites. Considering their small size and high surface-to-volume ratios, CDs can introduce a high density of defects, *i.e.* edges, into the composites and produce a great number of active sites for ORR.

3.3. Chemical compositions and surface structures of CD/rGO composites and directly doped rGO

Fourier transform infrared (FTIR) spectra (Figs. S6 and S7) indicate all prepared samples contain hydroxyl, carbonyl and epoxy oxygen groups, with respective absorption bands at around 3410, 1720 and 1400–1000 cm^{-1}.[31] It is noted N-doped samples have amide C—N absorption at 1450 cm^{-1}, different from the others, indicating that ethylenediamine reacts with carboxyl groups to form amide groups when N dopants are loaded into the CDs on the surface of rGO. Given the difficulty in discerning C—N/C—S and N—H/S—H groups from the strong background of C—O and O—H absorption, X-ray photoelectron spectroscopy (XPS) was performed to provide more information of chemical compositions and surface structures. XPS full survey spectra (Fig. S8) display the elemental compositions of all samples, and the corresponding concentrations of each element are listed in Table S1. It is clear that all samples are mainly composed of C and O elements, while N and S have been doped successfully into the CDs and rGO, respectively.

High-resolution XPS peaks of N 1s and S 2p are plotted (Fig. 3), and fitted (deconvolution) results are listed in Table S2. For N-CD/rGO, N1s peak can be deconvoluted to be pyrrolic N (400.7 eV), graphitic N (401.7 eV) and N oxide (402.7 eV) [39]. It is well-known that graphitic N plays a key role in catalyzing ORR, whilst the N oxide and the pyrrolic N contribute scarcely to ORR [13,40,41]. In N,S-CD/rGO, the graphitic N ratio in all N species approaches 56%, exceeding greatly those in the other cases, *i.e.* N-CD/rGO (38%), N,S-rGO (37%) and N-rGO (27%). For S-CD/rGO, S 2p spectrum of S-CD/rGO reveals two chemical states of S, namely thiophenic C—S—C (164.3 eV for $2p_{3/2}$ and 165.5 eV for $2p_{1/2}$) and oxidized C-SO_x-C (170.0 eV) [42]. Interestingly, the S 2p peak of N,S-CD/rGO shifts to larger binding energy, and this was ascribed to two new peaks representing benzothiadiazole-like S—N (166.0 eV for $2p_{3/2}$ and 167.2 eV for $2p_{1/2}$) [42]. Such a S—N structure has been regarded profitable for ORR [43], but it is not observed in N,S-rGO (Fig. 3h). Such a difference between N,S-CD/rGO and N,S-rGO may result from their doping processes, which will regulate their ORR performances. According to C 1s spectra (Figs. S9 and S10), N,S-CD/rGO and N,S-rGO have the largest C—N/C—S components of 26% and 27%, respectively. Considering the high dependence of the activity of carbon-based catalysts on the changed charge density of carbon atoms adjacent to heteroatoms [8,44], N,S-codoped samples have the highest density of ORR active sites.

To elucidate the function of CDs, their XPS spectra were also obtained and deconvoluted (Fig. S11). The full spectra of CDs in Fig. 11a show evident N and S peaks at ~400 eV and ~165 eV, respectively, demonstrating the successful doping of N and S elements in CDs. In Fig. S11b–d, the high-resolution C 1s XPS spectrum of N,S-CDs shows a larger fraction of C—N/C—S components

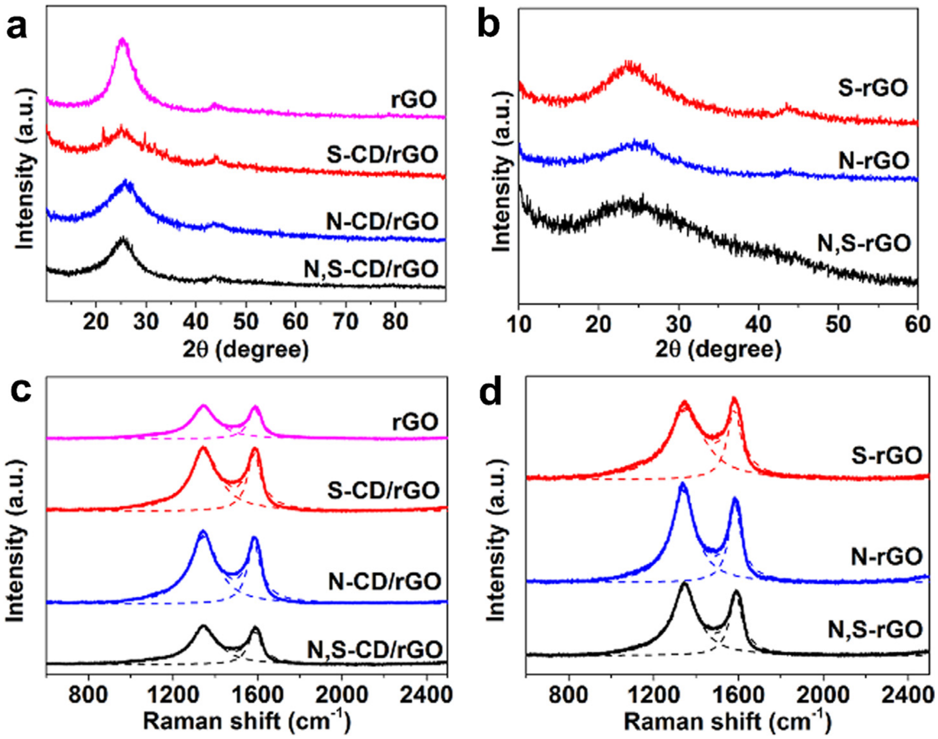

Fig. 2. (a, b) XRD patterns and (c, d) Raman spectra of all CD/rGO composites and the directly doped rGO samples. The I_D/I_G values were calculated by the area of the fitted peaks.

(~285.6 eV) than both N-CDs (~285.9 eV) and S-CDs (~285.3 eV), in accordance with the CD/rGO composites. The differences in binding energy of these samples are ascribed to the larger electronegativity of N than that of S. For N 1s spectra (Fig. S11e, f), the graphitic N fraction in N,S-CDs is larger than that in N-CDs, with a predominant pyrrolic N component. Regarding S 2p spectra (Fig. S11e, f), S—N structure exists exclusively in N,S-CDs, similar to that of N,S-CD/rGO. All these results indicate that the special structural properties of N,S-CDs were deposited in the N,S-CD/rGO composite, forming a good ORR catalyst.

3.4. Electrocatalytic activities of various rGO in ORR

In order to evaluate ORR performances of all samples, cyclic voltammetry (CV) measurements were conducted in O_2 or N_2 saturated 0.1 M KOH solution with a glassy carbon electrode on which samples were loaded with same mass. All CV curves of the doped rGO obtained in O_2 saturated KOH solution (Figs. S12 and S13) show well defined cathodic peaks corresponding to the reduction of oxygen, while that of free rGO is almost completely overlapped with the curve in N_2 saturated solution (Fig. S12d). The transformation from zero-activity of rGO to significant ORR activity of the doped rGO samples is undoubtedly ascribed to the heteroatom doping. On one hand, the directly doped rGO samples show inferior ORR performances to the corresponding CD/rGO composites (Table 1). For instance, N,S-CD/rGO has a more positive reduction potential and a larger current density than those of N,S-rGO. On the other hand, ORR catalyzing performance also depends on doped elements. Both N,S-CD/rGO and N,S/rGO samples exhibit more positive cathodic peak potentials and larger current densities than those of the individually doped counterparts. The mass ratio of CDs and rGO was maintained at 1:1 to achieve the best catalytic performance as mentioned above, and this is demonstrated by the comparison of CV curves of different N,S-CD/rGO samples with mass ratio ranging from 1:5 to 5:1, respectively. As shown in Fig. S14, the N,S-CD/rGO (1:5) curve shows almost no oxygen reduction peak, similar to that of rGO. When mass ratio of N,S-CDs and rGO was increased to 1:1, the ORR current becomes more evident. However, further increasing the proportion of N,S-CDs leads to a decrease in cathodic reduction peak, signifying that excess CDs may suppress the ORR activity. These results reveal that a mass ratio of CDs and rGO of 1:1 leads to the highest ORR activity.

To gain deep insights of ORR activity, linear sweep voltammetry (LSV) measurements were performed on a rotating-disc electrode at different rotation rates for all samples (Figs. 4a, S15 and S16). As shown in Fig. 4a and Table 1, N,S-CD/rGO exhibits the highest current density and the most positive half-wave potential (0.69 V vs. RHE) at a rotation rate of 1600 rpm. The kinetic current densities of all CD/rGO composites are higher than those of directly doped rGO samples (Fig. 4b). Because ORR activities of carbon-based materials are determined by the charge/spin distribution induced by heteroatom-doping, which is more active in edges than in basal planes, the higher ORR catalyzing activities of CD/rGO composites can be ascribed to the higher density of graphitic N at abundant edges of CDs. Notably, there are slight differences in their electron-transfer numbers between CD/rGO composites and directly doped rGO samples with same dopants (Fig. 4c and Table 1). However, N,S co-doped CD/rGO and rGO samples show quasi four-electron transfer pathways (3.90 for N,S-CD/rGO and 3.76 for N,S-rGO at 0.40 V vs. RHE), whilst the two-electron reduction pathway is dominant in the N or S solely doped samples. Such differences may be ascribed to the synergistic effects of S and N co-doping. In addition, the Tafel slope of N,S-CD/rGO (71 mV decade^{-1}) is lower than all the other samples, demonstrating the excellent catalytic activity of N and S co-doped CD/rGO, further suggesting a more favourable four-electron process over the N and S co-doped CD/rGO catalyst.

For comparison, Pt/C (20%) catalyst was tested under the same conditions. In Fig. S17b, the LSV curves of Pt/C at different rotation rates are illustrated and a half-wave potential of 0.83 V vs. RHE at

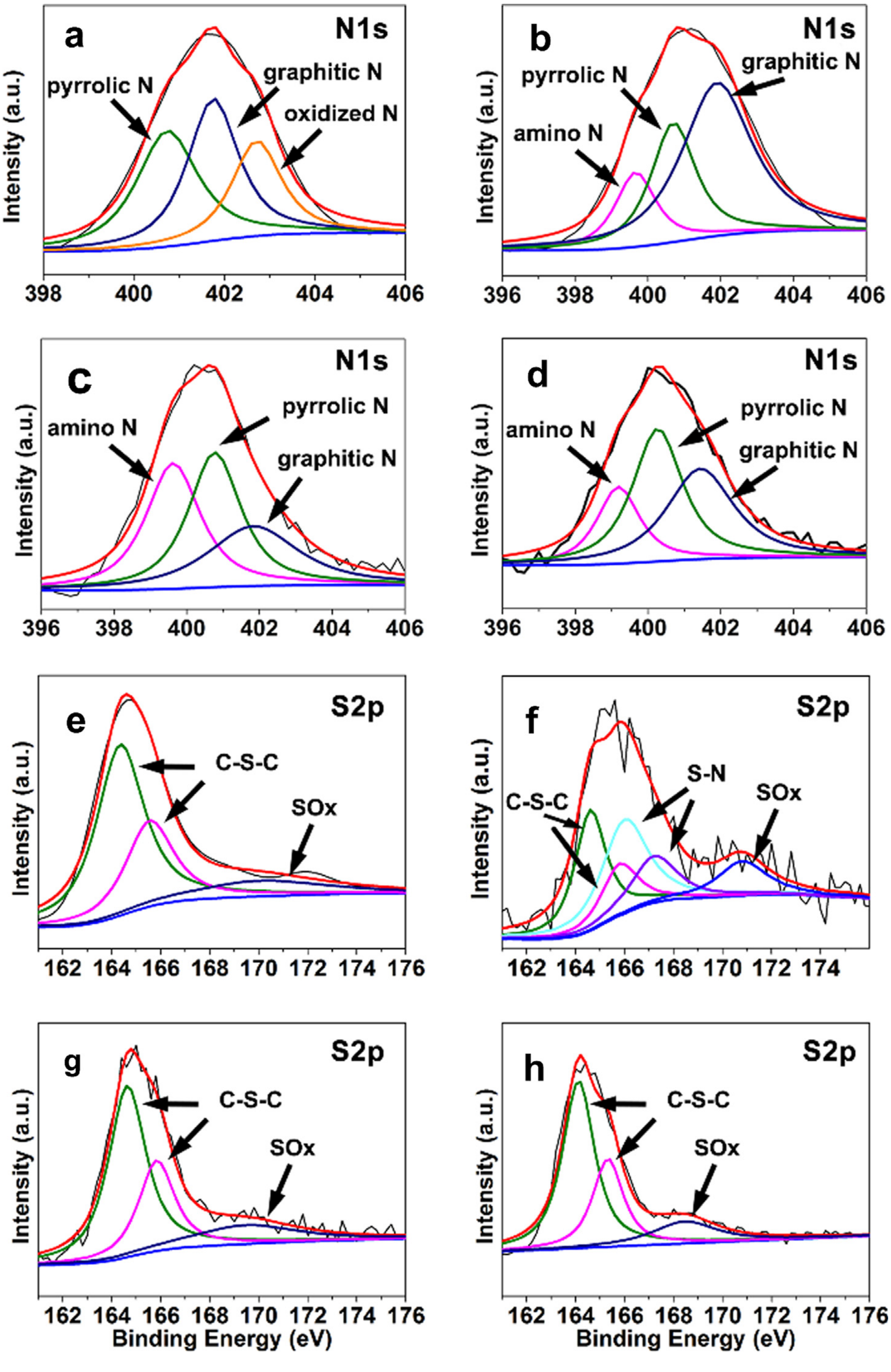

Fig. 3. High resolution N 1 s XPS spectra for (a) N-CD/rGO, (b) N,S-CD/rGO, (c) N-rGO and (d) N,S-rGO, respectively; and S 2p XPS spectra for (e) S-CD/rGO, (f) N,S-CD/rGO, (g) S-rGO and (h) N,S-rGO, respectively.

Table 1
Summaries of ORR performance on various catalysts in O_2-saturated 0.1 M KOH solution.

Catalysts	Half-wave potential (V vs. RHE)	Potential at 2 mA cm^{-2} (V vs. RHE)	Peak potential (V vs. RHE)	n
N,S-CD/rGO	0.69	0.71	0.68	3.90
N-CD/rGO	0.66	0.64	0.66	2.83
S-CD/rGO	0.68	0.67	0.66	2.89
N,S-rGO	0.67	0.66	0.63	3.76
N-rGO	0.66	0.62	0.62	2.89
S-rGO	0.66	0.63	Not observed	2.67

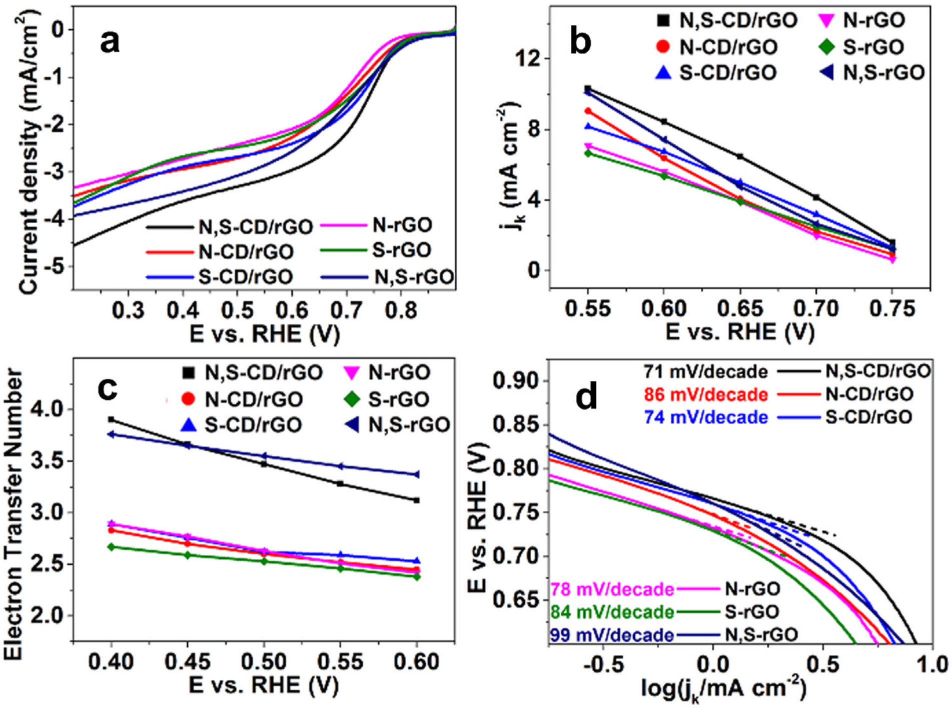

Fig. 4. (a) LSV curves at 1600 rpm for CD/rGO and doped rGO samples in O_2-saturated 0.1 M KOH solution, respectively. (b) and (c) The electron transfer numbers and kinetic current densities at different potentials calculated through K-L equation for all studied samples. (d) The Tafel plots of all studied samples.

1600 rpm is obtained. This means that N,S-CD/rGO is still inferior to the commercial Pt/C catalyst in terms of activity. The K-L plots of Pt/C are also depicted in Fig. S17c, and the electron transfer number of Pt/C at 0.4 V vs. RHE is calculated to be 3.92, close to that of N,S-CD/rGO. Furthermore, the Tafel slope of Pt/C (Fig. S17d) is determined to be 86.9 mV/dec, even larger than that of N,S-CD/rGO, which indicates N,S-CD/rGO has a good kinetic for ORR. Moreover, the long-term durability of N,S-CD/rGO was measured through chronoamperometric curves (Fig. S18a), and the results illustrate that the ORR current of N,S-CD/rGO decreases more slowly than that of commercial Pt/C. In addition, the tolerance ability towards methanol was tested in an aqueous solution containing 3 M of methanol, and the CV curve of N,S-CD/rGO in methanol shows a negligible shift versus the control without methanol (Fig. S18b), while the Pt/C (20%) shows poor methanol tolerance (Fig. S18c). All the above ORR tests confirm that N,S-CD/rGO presents the best electrocatalytic performance of all prepared samples.

3.5. Relationships between the catalyst features and their ORR catalyzing activities

ORR catalyzing activities of carbon-based electrocatalysts depend on the reactivity of their catalytic centers and the spatial effect of these active sites, in which the former is regulated by doped heteroatoms while the latter is related to spatial structures. Therefore, both the compositions and structures of our samples were examined to elucidate the mechanistic relationships between catalyst features and ORR performances.

With respect to composition, N and S dopants can lead to more positive charge densities and enhanced spin densities on the adjacent carbon atoms, which are preferable for both chemisorption and reduction of oxygen molecules [45]. Four kinds of N-containing samples (N,S-CD/rGO, N-CD/rGO, N,S-rGO and N-rGO) were prepared in the present study, of which the graphitic N is regarded as an active dopant widely. In Fig. 5a, these N-doped samples were studied to reveal the ORR activities as a function of their graphitic N fractions, where ORR activities are indicated by the potential at current density of 2 mA cm^{-2} ($E_{j=2}$) and the kinetic current density. The $E_{j=2}$ is selected rather than half-wave potential ($E_{1/2}$) because the limit currents are not evident in our LSV results, making it difficult to determine $E_{1/2}$. And the kinetic current density was calculated as an average of those at 0.75 V, 0.70 V and 0.65 V vs. RHE, respectively. These values were selected since they are in the kinetic controlled region according to the LSV curves, and their mean value is more representative to evaluate ORR kinetics. It is evident that an increase in graphitic N fraction of the samples leads to the increase in positive half-wave potential and kinetic current density. However, an exception can be observed in Fig. 5a, namely N,S-rGO shows better ORR performance than N-CD/rGO, which is inconsistent with their graphitic N fractions. Such a small deviation can be ascribed to the influence of S elements in N,S-rGO, because the N fraction cannot fully indicate the ORR activities. Therefore the influence of active S fractions on ORR activities is also illustrated in Fig. 5b, in which the ORR performances of the S-containing samples (N,S-CD/rGO, N-CD/rGO, N,S-rGO and S-rGO) were assessed in terms of total fractions of C—S—C and S—N. Obviously, these active S components also play an important role in ORR, showing a similar trend with that of $E_{1/2}$ and kinetic current density. Therefore, it can be concluded that the fractions of graphitic N and C—S—C/S—N structures are the key factors that affect ORR activities. Also, it is important to notice that the ORR activity is not solely determined by single N or S components. Therefore, when both graphitic N and active S components exist in one sample, a synergistic effects will endow the sample distinctive properties [46]. Fig. 5c reveals that the electron transfer numbers of N,S-CD/rGO and N,S-rGO are close to four. In contrast, all the singly-doped counterparts exhibit a two electron transfer pathway in ORR catalysis. Comparing the co-doped and the solely doped samples, the higher electron transfer numbers can be ascribed to the more active catalytic sites of dual-doped samples, since the increased charge and spin densities contribute

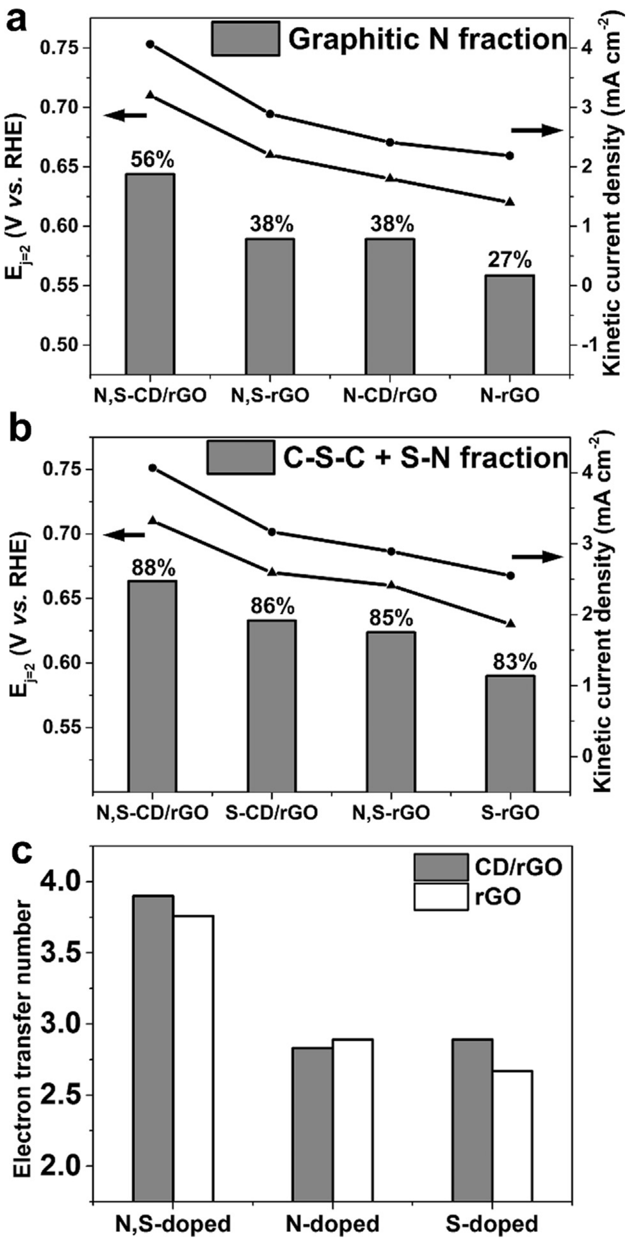

Fig. 5. (a) Graphitic N species fractions and corresponding potentials at current density of 2 mA cm^{-2} ($E_{j=2}$) as well as kinetic current densities of N-containing samples. (b) C—S—C and S—N total fractions and corresponding $E_{j=2}$ as well as kinetic current densities of S-containing samples. (c) Differences in electron transfer number between N,S-doped samples, and N or S doped samples.

significantly to ORR selectivity [35]. It has been proved that S dopants can thermodynamically improve the ORR performance of N-doped carbon allotropes by lowering the activation barrier for $O_2^* \rightarrow OOH^*$ step [47], well explaining the synergy of the S and N doping here.

With respect to structures, CD/rGO samples have three advantages compared to directly doped rGO, including high surface-to-volume ratios, abundant edges and active sites on the protuberant nanoparticles. Though the graphitic N is beneficial for ORR, there are some arguments that its locations inside the graphene sheets will hinder its exposure to oxygen molecules and reduce the electron conductivity [48]. In our zero-dimensional CDs, however, graphitic N locating on the surfaces of nanoparticles are much more active. In fact, the graphitic N at edges is proved to be more energy favourable than that in planes [49]. In terms of sulfur dopants, the thiophene-like C—S—C structure is preferentially located at edge sites, since it is difficult for S atoms to substitute sp^2 carbon atoms [4]. Therefore, the structure of CDs are favourable for the doping of S, which contributes greatly to the higher C—S—C/S—N fractions and ORR activities of CD/rGO composites in Fig. 5b. Scheme 2 illustrates that such structural advantages endow N,S-CD/rGO higher ORR reactivity than N,S-rGO, which is attributed to the hierarchical structure and more exposed active sites in N,S-CD/rGO [50].

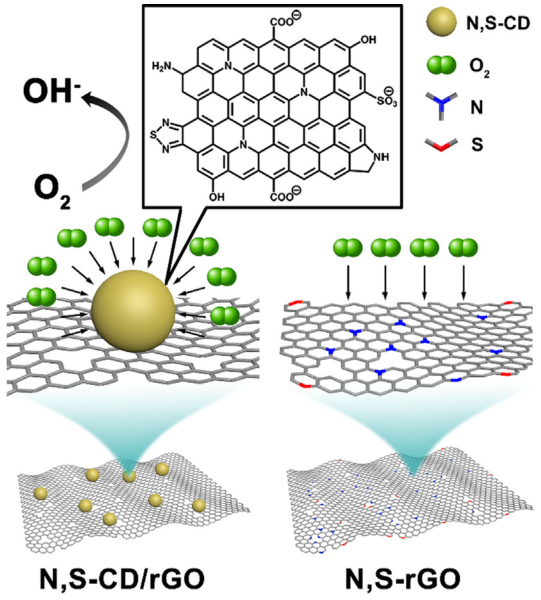

Scheme 2. Schematic illustration of the structures of N,S-CD/rGO and N,S-rGO, and the associated ORR pathways.

4. Conclusions

We prepared a series of carbon based ORR electrocatalysts through similar procedures for comparative investigations, and found both heteroatom-doping and substrate-constructing are key factors for their ORR activities. With respect to the heteroatom-doping, the effective components are graphitic N atoms and C—S—C/S—N species, which improve the half-wave potential and the current density. The synergistic effects of N,S co-doping endow the samples a preferred four-electron transfer pathway in ORR. With respect to substrate-constructing, active sites on CD surfaces exhibit better ORR activities than those in rGO planes, because the former locate in abundant edges/defects and have more access to oxygen molecules. As a result, N,S-CD/rGO exhibits the best ORR performance in all samples. Our present work provides valuable references for designing and constructing carbon-based catalysts, and proves CDs are a new class of cost-effective, stable, effective and adjustable catalysts for energy conversion applications.

5. Notes

The authors declare no competing financial interest.

Acknowledgements

This work was supported by the National Major Basic Research Program of China [grant number 2013CB934101]; the National Natural Science Foundation of China [grant number 21771039]; and the Shanghai Science and Technology Committee [grant number 16DZ2270100].

Appendix A. Supplementary material

Supplementary data to this article can be found online at https://doi.org/10.1016/j.jcis.2018.11.024.

References

[1] V.R. Stamenkovic, B. Fowler, B.S. Mun, G. Wang, P.N. Ross, C.A. Lucas, N.M. Markovic, Improved oxygen reduction activity on Pt$_3$Ni(111) via increased surface site availability, Science 315 (2007) 493–497.

[2] V.R. Stamenkovic, B.S. Mun, M. Arenz, K.J.J. Mayrhofer, C.A. Lucas, G.F. Wang, P. N. Ross, N.M. Markovic, Trends in electrocatalysis on extended and nanoscale Pt-bimetallic alloy surfaces, Nat. Mater. 6 (2007) 241–247.

[3] I.E.L. Stephens, A.S. Bondarenko, U. Grønbjerg, J. Rossmeisl, I. Chorkendorff, Understanding the electrocatalysis of oxygen reduction on platinum and its alloys, Energy Environ. Sci. 5 (2012) 6744–6762.

[4] D.-W. Wang, D. Su, Heterogeneous nanocarbon materials for oxygen reduction reaction, Energy Environ. Sci. 7 (2014) 576.

[5] J. Shui, M. Wang, F. Du, L. Dai, N-doped carbon nanomaterials are durable catalysts for oxygen reduction reaction in acidic fuel cells, Sci. Adv. 1 (2015) e1400129.

[6] X. Liu, L.M. Dai, Carbon-based metal-free catalysts, Nat. Rev. Mater. 1 (2016) 16064.

[7] R. Ma, X. Ren, B.Y. Xia, Y. Zhou, C. Sun, Q. Liu, J. Liu, J. Wang, Novel synthesis of N-doped graphene as an efficient electrocatalyst towards oxygen reduction, Nano Res. 9 (2016) 808–819.

[8] D. Guo, R. Shibuya, C. Akiba, S. Saji, T. Kondo, J. Nakamura, Active sites of nitrogen-doped carbon materials for oxygen reduction reaction clarified using model catalysts, Science 351 (2016) 361–366.

[9] P. Matter, L. Zhang, U. Ozkan, The role of nanostructure in nitrogen-containing carbon catalysts for the oxygen reduction reaction, J. Catal. 239 (2006) 83–96.

[10] M.W. Chung, C.H. Choi, S.Y. Lee, S.I. Woo, Dimensionality-dependent oxygen reduction activity on doped graphene: is graphene a promising substrate for electrocatalysis?, Nano Energy 11 (2015) 526–532

[11] C. Tang, Q. Zhang, Nanocarbon for oxygen reduction electrocatalysis: dopants, edges, and defects, Adv. Mater. 29 (2017) 1604103.

[12] G.-L. Tian, Q. Zhang, B. Zhang, Y.-G. Jin, J.-Q. Huang, D.S. Su, F. Wei, Toward full exposure of "active sites": nanocarbon electrocatalyst with surface enriched nitrogen for superior oxygen reduction and evolution reactivity, Adv. Funct. Mater. 24 (2014) 5956–5961.

[13] H.B. Yang, J.W. Miao, S.F. Hung, J.Z. Chen, H.B. Tao, X.Z. Wang, L.P. Zhang, R. Chen, J.J. Gao, H.M. Chen, L.M. Dai, B. Liu, Identification of catalytic sites for oxygen reduction and oxygen evolution in N-doped graphene materials: development of highly efficient metal-free bifunctional electrocatalyst, Sci. Adv. 2 (2016) e1501122.

[14] A.M. El-Sawy, I.M. Mosa, D. Su, C.J. Guild, S. Khalid, R. Joesten, J.F. Rusling, S.L. Suib, Controlling the active sites of sulfur-doped carbon nanotube-graphene nanolobes for highly efficient oxygen evolution and reduction catalysis, Adv. Energy Mater. 6 (2016) 1501966.

[15] H. Zhang, J. Chen, Y. Li, P. Liu, Y. Wang, T. An, H. Zhao, Nitrogen-doped carbon nanodots@nanospheres as an efficient electrocatalyst for oxygen reduction reaction, Electrochim. Acta 165 (2015) 7–13.

[16] I.Y. Jeon, S. Zhang, L. Zhang, H.J. Choi, J.M. Seo, Z. Xia, L. Dai, J.B. Baek, Edge-selectively sulfurized graphene nanoplatelets as efficient metal-free electrocatalysts for oxygen reduction reaction: the electron spin effect, Adv. Mater. 25 (2013) 6138–6145.

[17] X. Xu, R. Ray, Y. Gu, H.J. Ploehn, L. Gearheart, K. Raker, W.A. Scrivens, Electrophoretic analysis and purification of fluorescent single-walled carbon nanotube fragments, J. Am. Chem. Soc. 126 (2004) 12736–12737.

[18] J.-S. Wei, H. Ding, P. Zhang, Y.-F. Song, J. Chen, Y.-G. Wang, H.-M. Xiong, Carbon dots/NiCo$_2$O$_4$ nanocomposites with various morphologies for high performance supercapacitors, Small 12 (2016) 5927–5934.

[19] G.Q. He, Y. Song, K. Liu, A. Walter, S.S.W. Chen, S.S.W. Chen, Oxygen reduction catalyzed by platinum nanoparticles supported on graphene quantum dots, ACS Catal. 3 (2013) 831–838.

[20] H. Yu, R. Shi, Y. Zhao, G.I. Waterhouse, L.Z. Wu, C.H. Tung, T. Zhang, Smart utilization of carbon dots in semiconductor photocatalysis, Adv. Mater. 28 (2016) 9454–9477.

[21] C. Xu, Q. Han, Y. Zhao, L. Wang, Y. Li, L. Qu, Sulfur-doped graphitic carbon nitride decorated with graphene quantum dots for an efficient metal-free electrocatalyst, J. Mater. Chem. A 3 (2015) 1841–1846.

[22] J. Liu, S. Zhao, C. Li, M. Yang, Y. Yang, Y. Liu, Y. Lifshitz, S.-T. Lee, Z. Kang, Carbon Nanodot surface modifications initiate highly efficient, stable catalysts for both oxygen evolution and reduction reactions, Adv. Energy Mater. 6 (2016) 1502039.

[23] W.-J. Niu, R.-H. Zhu, H. Yan, H.-B. Zeng, S. Cosnier, X.-J. Zhang, D. Shan, One-pot synthesis of nitrogen-rich carbon dots decorated graphene oxide as metal-free electrocatalyst for oxygen reduction reaction, Carbon 109 (2016) 402–410.

[24] W. Wang, Y. Li, L. Cheng, Z. Cao, W. Liu, Water-soluble and phosphorus-containing carbon dots with strong green fluorescence for cell labeling, J. Mater. Chem. B 2 (2014) 46–48.

[25] X. Sun, C. Brückner, Y. Lei, One-pot and ultrafast synthesis of nitrogen and phosphorus co-doped carbon dots possessing bright dual wavelength fluorescence emission, Nanoscale 7 (2015) 17278–17282.

[26] D. Qu, Z. Sun, M. Zheng, J. Li, Y. Zhang, G. Zhang, H. Zhao, X. Liu, Z. Xie, Three colors emission from S, N co-doped graphene quantum dots for visible light $_H$2 production and bioimaging, Adv. Opt. Mater. 3 (2015) 360–367.

[27] Q. Li, S. Zhang, L. Dai, L.-S. Li, Nitrogen-doped colloidal graphene quantum dots and their size-dependent electrocatalytic activity for the oxygen reduction reaction, J. Am. Chem. Soc. 134 (2012) 18932–18935.

[28] Y. Li, Y. Zhao, H. Cheng, Y. Hu, G. Shi, L. Dai, L. Qu, Nitrogen-doped graphene quantum dots with oxygen-rich functional groups, J. Am. Chem. Soc. 134 (2012) 15–18.

[29] H. Fei, R. Ye, G. Ye, Y. Gong, Z. Peng, X. Fan, E.L.G. Samuel, P.M. Ajayan, J.M. Tour, Boron- and nitrogen-doped graphene quantum dots/graphene hybrid nanoplatelets as efficient electrocatalysts for oxygen reduction, ACS Nano 8 (2014) 10837–10843.

[30] H. Jin, H. Huang, Y. He, X. Feng, S. Wang, L. Dai, J. Wang, Graphene quantum dots supported by graphene nanoribbons with ultrahigh electrocatalytic performance for oxygen reduction, J. Am. Chem. Soc. 137 (2015) 7588–7591.

[31] H. Ding, J.-S. Wei, H.-M. Xiong, Nitrogen and sulfur co-doped carbon dots with strong blue luminescence, Nanoscale 6 (2014) 13817–13823.

[32] S. Zhu, Q. Meng, L. Wang, J. Zhang, Y. Song, H. Jin, K. Zhang, H. Sun, H. Wang, B. Yang, Highly photoluminescent carbon dots for multicolor patterning, sensors, and bioimaging, Angew. Chem. Int. Ed. 52 (2013) 3953–3957.

[33] W.S. Hummers, R.E. Offeman, Preparation of graphitic oxide, J. Am. Chem. Soc. 80 (1958) 1339.

[34] W. Niu, L. Li, X. Liu, N. Wang, J. Liu, W. Zhou, Z. Tang, S. Chen, Mesoporous N-doped carbons prepared with thermally removable nanoparticle templates: an efficient electrocatalyst for oxygen reduction reaction, J. Am. Chem. Soc. 137 (2015) 5555–5562.

[35] D. Higgins, P. Zamani, A. Yu, Z. Chen, The application of graphene and its composites in oxygen reduction electrocatalysis: a perspective and review of recent progress, Energy Environ. Sci. 9 (2016) 357–390.

[36] N. Jia, Q. Weng, Y. Shi, X. Shi, X. Chen, P. Chen, Z. An, Y. Chen, N-doped carbon nanocages: bifunctional electrocatalysts for the oxygen reduction and evolution reactions, Nano Res. 11 (2017) 1905–1916.

[37] J.S. Wei, H. Ding, Y.G. Wang, H.M. Xiong, Hierarchical porous carbon materials with high capacitance derived from Schiff-base networks, ACS Appl. Mater. Interfaces 7 (2015) 5811–5819.

[38] H. Ding, P. Zhang, T.Y. Wang, J.L. Kong, H.M. Xiong, Nitrogen-doped carbon dots derived from polyvinyl pyrrolidone and their multicolor cell imaging, Nanotechnology 25 (2014) 205604.

[39] M. Favaro, L. Ferrighi, G. Fazio, L. Colazzo, C. Di Valentin, C. Durante, F. Sedona, A. Gennaro, S. Agnoli, G. Granozzi, Single and multiple doping in graphene quantum dots: unraveling the origin of selectivity in the oxygen reduction reaction, ACS Catal. 5 (2015) 129–144.

[40] C. Zhang, R. Hao, H. Liao, Y. Hou, Synthesis of amino-functionalized graphene as metal-free catalyst and exploration of the roles of various nitrogen states in oxygen reduction reaction, Nano Energy 2 (2013) 88–97.

[41] T. Asefa, X. Huang, Heteroatom-doped carbon materials for electrocatalysis, Chem. Eur. J. 23 (2017) 10703–10713.

[42] M. Favaro, F. Carraro, M. Cattelan, L. Colazzo, C. Durante, M. Sambi, A. Gennaro, S. Agnoli, G. Granozzi, Multiple doping of graphene oxide foams and quantum dots: new switchable systems for oxygen reduction and water remediation, J. Mater. Chem. A 3 (2015) 14334–14347.

[43] Z. Luo, D. Yang, G. Qi, J. Shang, H. Yang, Y. Wang, L. Yuwen, T. Yu, W. Huang, L. Wang, Microwave-assisted solvothermal preparation of nitrogen and sulfur co-doped reduced graphene oxide and graphene quantum dots hybrids for highly efficient oxygen reduction, J. Mater. Chem. A 2 (2014) 20605–20611.

[44] X. Bai, Y. Shi, J. Guo, L. Gao, K. Wang, Y. Du, T. Ma, Catalytic activities enhanced by abundant structural defects and balanced N distribution of N-doped graphene in oxygen reduction reaction, J. Power Sources 306 (2016) 85–91.

[45] K. Gong, F. Du, Z. Xia, M. Durstock, L. Dai, Nitrogen-doped carbon nanotube arrays with high electrocatalytic activity for oxygen reduction, Science 323 (2009) 760–764.

[46] S. Bag, B. Mondal, A.K. Das, C.R. Raj, Nitrogen and sulfur dual-doped reduced graphene oxide: synergistic effect of dopants towards oxygen reduction reaction, Electrochim. Acta 163 (2015) 16–23.

[47] J.B. Zhu, K. Li, M.L. Xiao, C.P. Liu, Z.J. Wu, J.J. Ge, W. Xing, Significantly enhanced oxygen reduction reaction performance of N-doped carbon by heterogeneous sulfur incorporation: synergistic effect between the two dopants in metal-free catalysts, J. Mater. Chem. A 4 (2016) 7422–7429.

[48] S.F. Huang, K. Terakura, T. Ozaki, T. Ikeda, M. Boero, M. Oshima, J. Ozaki, S. Miyata, First-principles calculation of the electronic properties of graphene clusters doped with nitrogen and boron: analysis of catalytic activity for the oxygen reduction reaction, Phys. Rev. B 80 (2009) 235410.

[49] H. Kim, K. Lee, S.I. Woo, Y. Jung, On the mechanism of enhanced oxygen reduction reaction in nitrogen-doped graphene nanoribbons, Phys. Chem. Chem. Phys. 13 (2011) 17505–17510.

[50] E.J. Biddinger, U.S. Ozkan, Role of graphitic edge plane exposure in carbon nanostructures for oxygen reduction reaction, J. Phys. Chem. C 114 (2010) 15306–15314.